

The Third Option: Color Phase Curves to Characterize the Atmospheres of Temperate Rocky Exoplanets

DRAKE DEMING,^{1,2} ANDREW LINCOWSKI,^{3,2} LAURA KREIDBERG,⁴ MILES H. CURRIE,⁵ JEAN-MICHEL DESERT,⁶ GUANGWEI FU,⁷ JACOB LUSTIG-YAEGER,⁸ VICTORIA S. MEADOWS,^{3,9,2} AND IGNAS SNELLEN¹⁰

¹*Department of Astronomy, University of Maryland, College Park, MD 20742, USA*

²*NASA's Nexus for Exoplanet System Science, Virtual Planetary Laboratory Team, Box 351580, University of Washington, Seattle, WA 98195, USA*

³*SETI Institute, Carl Sagan Center, 339 Bernardo Ave, Suite 200, Mountain View, CA 94043, USA*

⁴*Max-Planck-Institut für Astronomie, Königstuhl 17, D-69117 Heidelberg, Germany*

⁵*NASA Goddard Space Flight Center, Greenbelt, MD 20771, USA*

⁶*Leibniz Institute for Astrophysics, An der Sternwarte 16, 14482 Potsdam, Germany*

⁷*Department of Physics and Astronomy, Johns Hopkins University, Baltimore, MD, USA*

⁸*JHU Applied Physics Laboratory, 11100 Johns Hopkins Rd, Laurel, MD 20723, USA*

⁹*Department of Astronomy and Astrobiology Program, University of Washington, Box 351580, Seattle, WA 98195, USA*

¹⁰*Leiden Observatory, Leiden University, Postbus 9513, 2300 RA, Leiden, The Netherlands*

ABSTRACT

Detecting and characterizing the atmospheres of rocky exoplanets has proven to be challenging for JWST. Transit spectroscopy of the TRAPPIST-1 planets has been impacted by the effects of spots and faculae on the host star. Secondary eclipses have detected hot rocks, but evidence for atmospheres has been difficult to obtain. However, there is a third option that we call color phase curves. This method will apply to synchronously rotating non-transiting planets as well as transiting planets. A color phase curve uses photometry at a long-IR wavelength near the peak of the planetary thermal emission (e.g., 21 microns) divided by photometry at a shorter wavelength where the star dominates more strongly (e.g., 12 microns). We avoid wavelengths having potentially strong molecular absorption (e.g., 15 microns) to minimize degeneracies in the color phase curve, and we aim to detect and characterize the planetary atmosphere via its longitudinal heat transfer. The ratio of two wavelengths observed nearly simultaneously is designed to isolate thermal emission from the planet, discriminate against the star, and largely cancel instrumental systematic effects. Moreover, we show that invoking mass-radius relations, and using self-consistent physical models, will permit the longitudinal heat transfer to be measured independent of the orbital inclination. Radial velocity surveys are detecting many new exoplanets, including temperate rocky worlds with Earth-like masses. Most of those planets will not transit, but color phase curves have the potential to detect and characterize their atmospheres.

1. INTRODUCTION

Detecting and characterizing the atmospheres of rocky exoplanets is a scientific priority (Charbonneau & Gaudi 2018). This quest has been challenging for JWST. Two observational techniques applied to transiting systems have dominated these attempts: transit and eclipse spectroscopy. Transit spectroscopy of rocky planets has produced only hints of spectral features, and secondary eclipses have been broadly consistent with bare rocky surfaces (Greene et al. 2023; Zieba et al. 2023; Xue et al. 2024; Weiner Mansfield et al. 2024; Alderson et al. 2024; Lustig-Yaeger et al. 2023; Kirk et al. 2024; Scarsdale et al. 2024; Moran et al. 2023; May et al. 2023; Lim et al. 2023; Gressier et al. 2024; Cadieux et al. 2024; Damiano et al. 2024; Ducrot et al. 2025; Radica et al. 2025; Glidden et al. 2025; Espinoza et al. 2025; Gillon et al. 2025, reviewed by Kreidberg & Stevenson 2025, and Espinoza & Perrin 2025). Moreover, transit spectroscopy is

sensitive to interference by the Transit Light Source effect (Rackham et al. 2018), notably in the TRAPPIST-1 planets (e.g., Piaulet-Ghorayeb et al. 2025). Thin atmospheres are possibly detected in some cases (Greene et al. 2023), and ultra-hot rocky planets can have atmospheres from magma oceans (Hu et al. 2024; Teske et al. 2025). Nevertheless, new observational approaches to this problem are needed.

In this paper, we develop and advocate a third observational option for temperate rocky planets, that we call color phase curves (hereafter CPC). CPCs are based on a ratio of filter photometry at two different wavelengths observed nearly simultaneously. For temperate planets, an optimal strategy is to choose one wavelength near the peak of a temperate planet's thermal emission (e.g., $21\text{ }\mu\text{m}$) and another wavelength that is relatively more sensitive to the star (e.g., $12\text{ }\mu\text{m}$). The ratio of fluxes observed at those two wavelengths has great potential to isolate thermal emission from temperate planets, discriminate against the star, and cancel instrumental systematics.

To our knowledge, it was Stevenson et al. (2020) who first proposed exploiting the infrared emission of temperate planets at long IR wavelengths, and Galuzzo et al. (2020) who emphasized using JWST's MIRI photometry at $21\text{ }\mu\text{m}$. Our CPC concept expands on those ideas by using the ratio of $21\text{- to }12.8\text{ }\mu\text{m}$, by considering the advantages for stellar contamination (§3.1), and exploring how to infer the day-to-night temperature difference without knowing the orbital inclination (§6). Although JWST's long wavelength sensitivity and low thermal background are well suited to our proposed CPC method, it has not been attempted in practice. In that respect, JWST is arguably under-utilized for temperate exoplanets in spite of a healthy oversubscription status. Specifically, the MIRI $21\text{ }\mu\text{m}$ filter has yet to be used for temperate rocky exoplanets, but modeling predictions (Kreidberg & Loeb 2016; Galuzzo et al. 2021) have been encouraging.

1.1. *Organization of This Paper*

We outline the CPC principle in §2.1, and we point out that it applies to non-transiting planets as well as transiting planets. §3.1 describes how the long thermal wavelengths allow very effective discrimination against star spots and faculae, and §3.2 describes the effect of stellar flares. §3.3 discusses the potential for mitigation of instrumental systematic effects. §4 and §5 simulate a detection of the atmosphere of the archetype temperate non-transiting rocky exoplanet Proxima Centauri b. Beyond the detection, §6 describes how to measure the longitudinal heat redistribution in the atmosphere, in spite of uncertainty in the inclination of the orbit. §7 describes the potential for CPCs to be applied to a larger sample of nearby non-transiting planets. § 8 summarizes our results.

2. COLOR PHASE CURVES (CPC)

2.1. *Principle of CPC*

Our goal in this paper is to develop the CPC principle, and illustrate how it applies to a sample of planets, including non-transiting rocky planets. Given that non-transiting planets are more common than transiting ones, it is likely that CPC in practice will be primarily a non-transiting method. CPC relies on the fact that the flux from a temperate exoplanet, relative to its star, will peak at a long IR wavelength. In that respect CPC is similar to the Planetary Infrared Excess method proposed by Stevenson et al. (2020) (also, see Lustig-Yaeger et al. 2025 and Limbach et al. 2024), but we place more emphasis on the Rayleigh-Jeans regime (§3.1), and we discuss how the magnitude of heat transfer can be determined without knowing the orbital inclination (§6). CPC requires that we know what longitudes on the planet are contributing to our measurements at every observed time. That is easiest to do if we are confident that the planet is synchronously rotating, or at least in a lower order resonance such as 3:2 (Ribas et al. 2016).

The scientific potential of infrared phase curves for non-transiting planets has long been known (Seager & Deming 2009; Selsis et al. 2011; Maurin et al. 2012). Seager & Deming (2009) pointed out that a phase curve having low amplitude can be interpreted as the consequence of longitudinal heat transport by an atmosphere, whereas a synchronously-rotating rocky planet lacking an atmosphere would be expected to have a phase variation of large amplitude (depending on the orbital inclination). Selsis et al. (2011) described how the phase curve amplitude varies with wavelength as a consequence of the composition, pressure, and temperature of the atmosphere. Maurin et al. (2012) investigated how multi-wavelength phase curves can be analyzed to constrain the planet's radius, albedo, and orbital inclination. Swain et al. (2025) discussed how comparing phase curves at different wavelengths can inform us of atmospheric properties. However, to our knowledge there is no discussion in the literature that addresses a phase curve measurement using the ratio of two wavelengths observed nearly simultaneously, especially at the long IR wavelengths we discuss in this paper.

We envision detecting and characterizing the atmospheres of temperate rocky planets by inferring their heat transport (or lack of it), following the principle of [Seager & Deming \(2009\)](#). Our current formulation of CPC requires that the planet be synchronously rotating, and also we are interested in temperate planets. Because synchronous planets are often close to their host star, they will tend to be hotter than an Earth-like temperature unless the host star has low luminosity. Thus, temperate rocky planets orbiting M-dwarf stars are the natural targets of the CPC method. We choose two wavelength bands that are dominated by continuum radiation (12.8- and 21 μm), and we avoid potentially strong absorptions such as the 15 μm carbon dioxide band. The reason for that choice is to maximize the amplitude of the CPC, and to avoid possible degeneracies between phase curve parameters and atmospheric composition ([Ducrot et al. 2025](#)).

In general, we will not know the orbital inclination of a non-transiting target planet, but in §6 we demonstrate that at least an approximate measurement of the longitudinal heat redistribution can be made without knowing the orbital inclination.

2.2. *Observational Methodology*

Transiting exoplanet observers have ample experience with phase curves, and the normal observational procedure follows [Knutson et al. \(2007\)](#) by obtaining a continuous uninterrupted time series of observations. Not only do continuous observations densely sample orbital phases, but they also help to deal with possible drifts in instrumental sensitivity. In principle, a phase curve could be sampled only at a small number of discrete times. If those samples are scheduled independently and interleaved with other observations, there is significant risk that the phase curve will be affected by uncorrectable variations in instrumental sensitivity. Nevertheless, space-borne instrumentation is often very stable, and (for example) [Crossfield et al. \(2010\)](#) were able to use some discrete samples in their *Spitzer* phase curve of Upsilon And b. Also there is evidence that MIRI filter photometry on JWST is stable, or only very slowly varying, on the long orbital time scales of temperate planets ([Gordon et al. 2025](#)).

We envision that a CPC of a temperate rocky exoplanet would rely on discrete sampling at strategically selected times, with consecutive observations of the two photometric bands in each visit. The observations would use broad-band filter photometry to maximize the number of observed photons, and risk of saturation is reduced because stars are increasingly fainter as long IR-wavelength increases. Radial velocity results are often sufficiently precise ([Suárez Mascareño et al. 2025](#)) to allow CPC photometric observations to be scheduled near anticipated peaks and valleys in the phase curve, enhancing the precision for measurement of the amplitude. Most important, CPC measures the integrated light of the exoplanet system (planet+star) as a *ratio* of the fluxes in two wavelength bands. Those two bands would be observed consecutively in the same visit, using the same detectors. Although there is no guarantee that instrumental effects will strictly cancel in the ratio, the observations can be designed to facilitate that cancellation as much as possible (e.g., §3.3).

3. SOURCES OF INTERFERENCE

3.1. *Star Spots and Faculae: Advantage of the Rayleigh-Jeans Limit*

[Seager & Shapiro \(2024\)](#) point out that the nature of the Planck function facilitates transit spectroscopy at long thermal wavelengths. Emergent spectra of stars are not necessarily formed in local thermodynamic equilibrium (LTE), i.e. the source function for the emergent spectrum is not necessarily the Planck function. Non-LTE effects are well known in strong resonance lines, and in stars having low surface gravity ([Asplund 2005](#)). Even some transitions in the thermal infrared spectra of the Sun deviate significantly from LTE ([Carlsson et al. 1992](#)). Nevertheless, LTE is a good approximation for most of the thermal IR spectra of M-dwarf stars ([Seager & Shapiro 2024](#)), especially in the continuum. Moreover, line structure is weak at long IR wavelengths, so the stellar continuum dominates filter photometry. Thus, the properties of the Planck function are central to flux variations in the stellar hosts of temperate rocky planets as observed using filter photometry.

Because CPC uses a *ratio* of two wavelengths, stellar variations are potentially better behaved for CPC than [Seager & Shapiro \(2024\)](#) discuss for transit spectroscopy. The issue is to what extent variations in the stellar flux will occur due to variable contributions of spots and faculae as they form and evolve, and as the star rotates. In the Rayleigh-Jeans limit, the Planck function (B_λ) becomes:

$$B_\lambda(T) = 2kT/\lambda^4 \quad (1)$$

Consider a star with photospheric temperature T_p and star spot temperature $T_s = T_p - \delta T$. Let the solid angle subtended by the star spot (as observed by JWST) be ϵ , in units where the solid angle subtended by the JWST-facing stellar disk is unity. Then the flux measured by JWST for the spotted star is:

$$F_{\text{spotted}} = 2kc[(1 - \epsilon)T_p + \epsilon T_s]/\lambda^4, \quad (2)$$

and:

$$F_{\text{unspotted}} = 2kcT_p/\lambda^4 \quad (3)$$

Thus,

$$F_{\text{spotted}}/F_{\text{unspotted}} = 1 - \epsilon(\delta T/T_p) \quad (4)$$

Hence in the Rayleigh-Jeans limit, the flux from a spotted star relative to the flux from the same star without spots, is independent of wavelength. (The same statement applies to faculae, or a mixture of spots and faculae, because the equations are similar.) The CPC will be potentially contaminated by variable spot coverage, and the CPC measurements are relative in time. Therefore, the potential contamination of the CPC varies similarly as the ratio of spotted star to unspotted star, and it is independent of wavelength. Thus, in the Rayleigh-Jeans limit, spatial variations in stellar temperature have no effect on CPCs.

The reason that wavelength cancels in $F_{\text{spotted}}/F_{\text{unspotted}}$ is because the Planck function becomes linear in temperature, which allows the wavelength dependence to be separated as a multiplicative factor, thus canceling in the flux ratio. At short wavelengths, temperature and wavelength appear in the Planck function together in an exponential, and therefore the wavelength dependence does not factor out, and does not cancel in the flux ratio.

That being said, real measurements will not strictly be in the Rayleigh-Jeans limit, which applies at infinite wavelength. Choosing 12.8- and 21 μm MIRI filters, we used model atmospheres to calculate the effect for real observations. We consider the case of an M-dwarf star ($T_{\text{eff}} = 3000\text{ K}$), and a star spot temperature deficit of $\delta T = -200\text{ K}$ (Savanov & Dmitrienko 2019). We use a spot area coverage consistent with the amplitude of the optical rotational light curve of Proxima Centauri b (Figure 7 of Wargelin et al. 2024). We use Phoenix model atmospheres for both the photosphere and the star spot, and we integrate their emergent fluxes over the bandpasses of the MIRI filters and including the wavelength-dependent detector response. The results are tabulated in Table 1, and we see that in this case the difference in the flux ratio between the two wavelengths is 634 parts-per-million. Although that is larger than the flux ratio from many temperate rocky exoplanets, it is much less than would prevail at optical wavelengths. Also, many M-dwarfs rotate slowly (Newton et al. 2018; Popinchalk et al. 2021), and CPCs can exploit different time scales for stellar rotation versus the exoplanet's orbital period, as we illustrate in §5.

Table 1. Example of the wavelength dependence of the ratio between the flux of a spotted star divided by the flux from the same star without spots. The star is an M-dwarf with $T_{\text{eff}} = 3000\text{ K}$, with a star spot whose projected area is 0.08 of the total stellar disk's projected area. The temperature deficit of the star spot is 200 K. The ratio of spotted-to-unspotted flux is almost equal at the two MIRI filter wavelengths (integrated over the bandpasses); the difference in the ratio is 634 ppm.

Wavelength (μm)	$F_{\text{spotted}}/F_{\text{unspotted}}$
12.8	0.990855
21	0.990221

3.2. Stellar Flares

Stellar exoplanet hosts can exhibit flares at infrared wavelengths. For example, Seager & Deming (2009) encountered a flare in their exploratory observations of GJ 876, and Gillon et al. (2025) found multiple flares on TRAPPIST-1. The advantages of the Rayleigh-Jeans regime are not relevant to flares, because their mid-IR emission is not thermal (Kaufmann et al. 2004). In the case of Proxima Centauri, flares occur during about 7% of observations (Vida et al. 2019). Fortunately, flares are easily recognized by their sharp rise time (Seager & Deming 2009; Yang et al. 2025). To the extent that they can be detected in CPC data, they can be either corrected by model fitting (Gillon et al. 2025), or zero-weighted using digital filters. However, it is possible that a population of low-amplitude flares may be more difficult to identify and correct than are large events. This is a topic that needs additional investigation.

3.3. The Instrument

Observing a color, i.e. two wavelengths, can facilitate the mitigation of instrumental systematic errors that often originate in the detectors. We anticipate that the ratio between two wavelengths can be measured more precisely than photometry in a single wavelength, because the same detector can be used for both wavelengths (e.g., JWST/MIRI has one detector array for filter imaging). Different wavelengths will not illuminate the detector in the same way, because of wavelength-dependent diffraction. That mismatch can be at least partially compensated by dithering. Nevertheless, there will probably be residual effects wherein detector sensitivity does not cancel perfectly between the two wavelengths. Hence we must consider how those effects will impact the CPC.

Changes in detector sensitivity during transit and eclipse observations have been familiar to exoplanet observers for two decades. For example, [Deming et al. \(2006\)](#) found a strong change in detector sensitivity (a "ramp") during one of the earliest secondary eclipse observations using Spitzer. The JWST detectors are better in that regard (e.g., [Fu et al. 2024](#)), but changes in detector sensitivity still occur. Those changes can be grouped into short-term changes that occur during an observational visit, and long term changes that occur between visits.

Short-term changes in detector response include effects of charge-trapping and persistence. However, these effects in JWST/MIRI photometry stabilize quickly for bright sources, as recently demonstrated by [Connors et al. \(2025\)](#). That behavior is consistent with the experience of Spitzer observers, who sometimes observed a bright extended source immediately prior to a transiting system in order to 'pre-flash' and stabilize the detector ([Knutson et al. 2011](#)). Long-term changes could also occur, investigated by [Gordon et al. \(2025\)](#), and are greater at $21\text{ }\mu\text{m}$ than at $12.8\text{ }\mu\text{m}$. Fortunately, [Gordon et al. \(2025\)](#) found that long-term changes decay exponentially, and we are now far from their starting epoch (Julian date $t_0 = 2459720$). From their fitted curves, we expect a change in relative detector response (21 vs. $12.8\text{ }\mu\text{m}$) that is insignificant for the purpose of CPC observations.

4. AN EXAMPLE: DETECTING THE ATMOSPHERE OF PROXIMA CENTAURI B

To illustrate how CPC would work in practice, we use the example of Proxima Centauri. This system has two planets: b and d. Proxima b ([Anglada-Escudé et al. 2016](#)) is within the star's habitable zone and temperate ($T \sim 218\text{ K}$), and rocky with 90% probability ([Bixel & Apai 2017](#)) - especially given the recently-inferred orbital inclination of 47-degrees ([Klein et al. 2021](#); [Suárez Mascareño et al. 2025](#)). An orbital eccentricity $e < 0.1$ ([Suárez Mascareño et al. 2025](#)) makes it likely to rotate synchronously. It does not transit ([Jenkins et al. 2019](#); [Gilbert et al. 2021](#)). Proxima d ([Suárez Mascareño et al. 2020, 2025](#)) is smaller in mass, radius, and orbital distance, also rocky, and likely synchronous. Table 2 summarizes the basic properties of Proxima's planets, but those numbers are for context only - we calculated emergent fluxes for specific models as described in §5. A third planet ('c') has been reported ([Damasso et al. 2020](#)), but is still uncertain ([Artigau et al. 2022](#)), so we do not include it here.

Table 2. Parameters of the Proxima system. Period is orbital for the planets and rotational for the star, all in days. Radii are in Suns for the star, and Earths for the planets. Sources are [1: [Boyajian et al. \(2012\)](#)], [2: [Suárez Mascareño et al. \(2020\)](#)], [3: [Mann et al. \(2015\)](#)], [4: calculated in this work using the empirical mass-radius relation from [Müller et al. \(2024\)](#)].

	Star	'b' planet	'd' planet
Temperature	$3050 \pm 100\text{ K}$ [1]	$218 \pm 18\text{ K}$ [2]	$282 \pm 23\text{ K}$ [2]
Mass	0.122 ± 0.002 [3]	1.44 ± 0.21 [2]	0.357 ± 0.072 [2]
Radius	0.141 ± 0.021 [1]	1.12 [4]	0.77 [4]
Period	83.2 ± 1.6 [2]	11.18465 ± 0.00053 [2]	5.12338 ± 0.00035 [2]

Based on the stellar and orbital parameters in Table 2, we calculated CPCs for the Proxima system ('b'+d' planets) using several models. First, we used the 'Toy Climate Model' from [Kreidberg & Loeb \(2016\)](#), applying that model also to the 'd' planet by scaling the 'b' phase curve to the temperature and radius of 'd'. For the 'b' planet, we also include the results from the GCM calculation of [Galuzzo et al. \(2020\)](#). Those authors do not tabulate their full phase curves, but their Figure 8 appears very sinusoidal, with a shape similar to the toy model from [Kreidberg & Loeb \(2016\)](#). We therefore include the GCM result by scaling the toy model to the GCM amplitudes and orbital inclination, using Tables 2 and 3 in [Galuzzo et al. \(2020\)](#) to mimic a GCM version of the CPC for planet 'b'.

CPCs for the sum of both planets at an orbital inclination of 47-degrees ([Suárez Mascareño et al. 2020](#)) are shown in Figure 1. The toy models for 'b' and 'd' in this case are for zero heat redistribution, and a Bond albedo of $0.1, =$

dark, hot rocks. The GCM amplitude from [Galuzzo et al. \(2020\)](#) corresponds to a Bond albedo near 0.3, = Earth-like. [Galuzzo et al. \(2020\)](#) do not quote the degree of bolometric heat redistribution produced by their GCM, but from the contrast in their phase curve (maximum versus minimum), we estimate the redistribution to be approximately 40% (on a scale where complete redistribution in longitude is 100%).

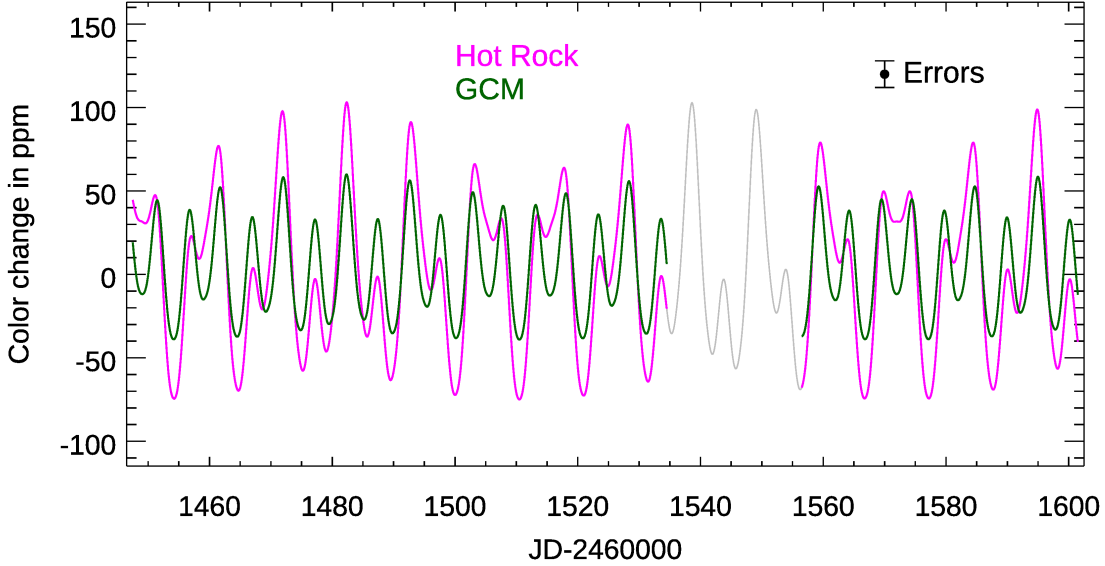


Figure 1. Color phase curves (CPCs) for the sum of planets 'b' and 'd' in the Proxima Centauri system. The CPC is the ratio of the flux in the $21\ \mu\text{m}$ to $12.8\ \mu\text{m}$ JWST/MIRI filters, normalized to the stellar flux, with the median value subtracted from the normalized ratio. The CPCs are the sum of both planets, and are shown here for the 2027 visibility period for JWST (lighter when not visible). Two cases are shown: using a hot rock model for 'b', and a GCM (see text). Planet 'd' is modeled as a hot rock in both cases.

Figure 1 includes the 'd' planet as a hot rock, added to both the toy model and the GCM for planet 'b'. We used a Phoenix model for the star, and we integrated the planetary and stellar models over the bandpasses of the MIRI 12.8- and $21\ \mu\text{m}$ filters, including variations in the detector response with wavelength. The CPCs for the two planets come in and out of phase with each other, with a total peak-to-peak variation (both planets) of ~ 160 ppm for the toy model applied to 'b', and ~ 100 ppm using the GCM model for b ('d' is a hot rock in both cases). We envision a series of observations (described in §5), wherein the total exposure time ($12.8\ \mu\text{m} + 21\ \mu\text{m}$) equals 3.5 hours per each of 25 visits, and we use the MIRI Exposure Time Calculator to calculate the photon-limited noise for each visit (= 8 parts-per-million).

We explored additional models for both the 'b' and 'd' planets, using the two-column formulation described by [Lincowski et al. \(2023\)](#). We emphasize that these models are not intended as a prediction for this planetary system based on first principles; rather, they are plausible models to test the detectability of this system. The two-column method adopts day and night-side atmospheric columns, and transport between them is calculated for each vertical layer using the 3D primitive equations. A key advantage of this method is that radiative transfer can be treated more completely than is often possible using GCMs. Radiative transfer was calculated using the Spectral Mapping Atmospheric Radiative Transfer code (SMART). SMART uses a multi-stream, multi-scattering algorithm at high spectral resolution ([Meadows et al. 2018](#); [Meadows & Crisp 1996](#)). The hemispherically-averaged day side column does not spatially resolve the narrow substellar region ([Gillon et al. 2025](#)), hence these models probably underestimate the phase curve amplitudes and thereby provide conservative estimates of detectability.

Our two-column model for the 'b' planet is an Earth-like atmosphere with the volume mixing ratio of carbon dioxide equal to 280 parts-per-million. Figure 2 shows the CPC for that model; it has an albedo of 0.3, and 35% of the incident stellar energy transported to the night side. The 'b' amplitude from the two-column model is less than the GCM model due to the hemispherical averaging mentioned above (also, see § 5), but the Bond albedo and the heat circulation are similar. Figure 2 also uses a two-column model for the 'd' planet. That 'd' model is a "Dune"-like

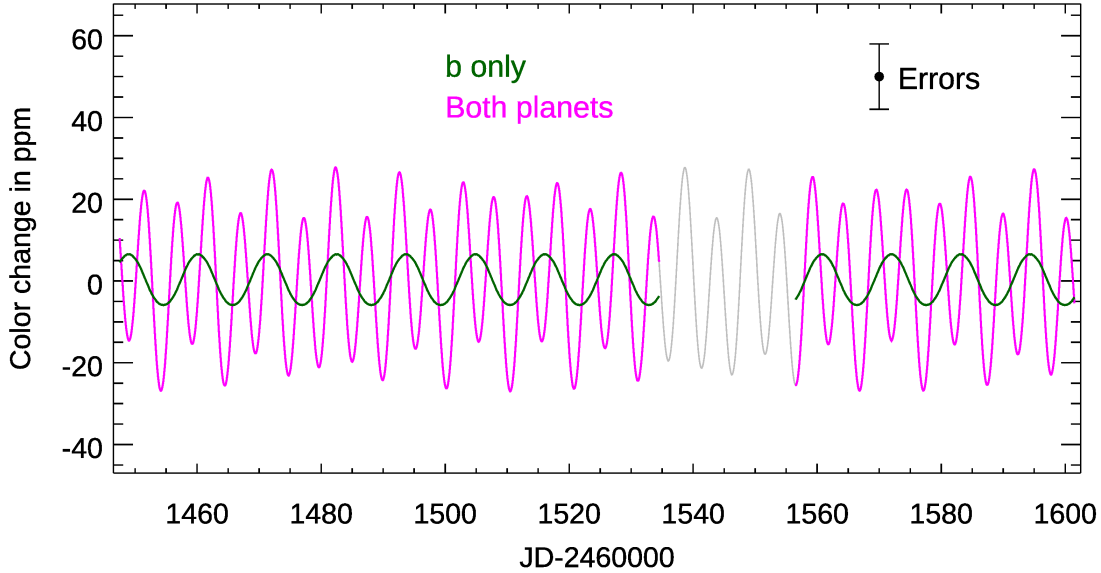


Figure 2. Color phase curves (CPCs) for planets 'b' and 'd' in the Proxima Centauri system, as in Figure 1, except that the CPC for the 'b' planet is here also plotted separately, in addition to being summed with 'd'. Both planets are represented by the two-column model of Lincowski et al. (2023) (see text for description).

planet having Earth-like atmospheric gases except a 10% relative surface humidity, no clouds, and albedo = 0.1. It has no transport to the night side.

5. MEASURING THE PHASE CURVE AMPLITUDE

The first inference that can be made from CPC data is a retrieval of the separate amplitudes of the CPC for each exoplanet in the system that contributes significantly. We have simulated this process for the Proxima system's CPCs shown in Figures 1 and 2. The radial velocity data (Suárez Mascareño et al. 2025) are sufficiently precise to enable observations to be selectively scheduled at the times where peaks and valleys are expected to occur in the total CPC. We simulated 50,000 sets of observational data, all based on the same targeted observational windows, but with the exact time varying randomly within each ± 0.5 day window, to mimic the scheduling constraints of real observations. We create the data samples from the modeled CPCs, summing both the 'b' and 'd' planets, and adding Gaussian random noise to each observation with a standard deviation of 8 ppm. We also varied the planetary orbital inclinations (taken to be coplanar) when generating each set of data, and also their orbital periods, using Gaussian distributions corresponding to the current observational uncertainties (Table 2). In addition to the total CPC due to planets 'b' and 'd', we add stellar variation that is modeled as sinusoidal at the 83.2-day rotational period, and having a peak-to-peak amplitude of 634 ppm in the 21- versus 12.8 μm color (§3.1, and Table 1).

For each set of simulated data, we solve for the amplitudes of the CPCs for 'b' and 'd', and the amplitude of stellar variation, using multi-variate linear regression. In real data, it is possible that the stellar variation could be at least partially inferred from the absolute fluxes (Table 1), but our regression solutions do not attempt that. The regression solutions assume that the planetary orbital periods are always equal to the current best-estimate values (although we vary them in the simulated data), and the regression solves for their amplitudes. Since the regression does not know the orbital inclination, it adopts 47-degrees (Klein et al. 2021) in all cases; consequently the retrieved amplitudes are degenerate with the variations in inclination that are included in different realizations of the data.

Figure 3 shows the corner plot for the data simulations corresponding to Figure 1. The amplitude of the 'd' curve is degenerate with the orbital inclination as expected. The amplitude for 'b' however, is less degenerate with inclination. We attribute that to the nature of the day- versus night-side temperature contrast that is much less for 'b' because of the presence of an atmosphere with heat redistribution. The retrieved median amplitude of 'd' is 75.4 ± 8.6 ppm, and for 'b' is 30.5 ± 7.0 ppm, where the uncertainties include degeneracy with the orbital inclination. The input values

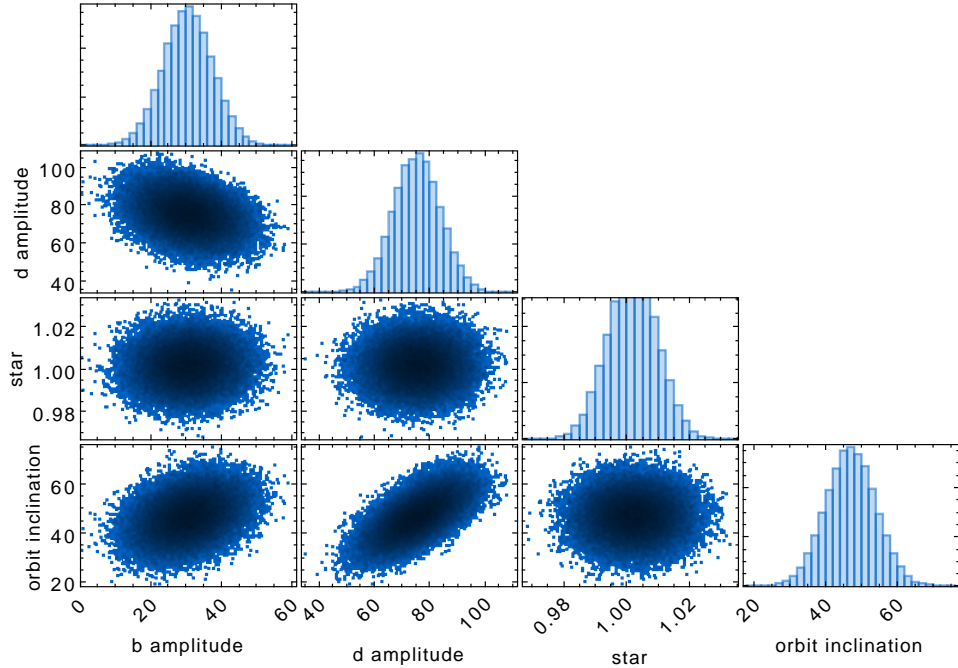


Figure 3. Corner plot for multi-variate linear regression results from 50,000 sets of simulated CPC data for the Proxima system. Each data set is based on 25 observations of the CPCs shown in Figure 1, with 8 ppm error bars. The planets are taken to be coplanar, and the regression solves for the CPC amplitudes of planets 'b' and 'd', as well as the amplitude of stellar variation. The orbital inclination is varied for each simulated dataset, with the amplitude of variations corresponding to the current observational uncertainties (Table 2).

are 77 and 29 ppm, respectively. Had we used the toy model for 'b' (a "hot rock") with no redistribution of heat, the amplitude would be 114 ppm - a high significance detection. We conclude that summed CPCs for two planets in the Proxima system can be successfully decomposed into their individual amplitudes, if the 8 ppm precision that we project for the color measurements can be achieved. Also, Figure 3 shows essentially no degeneracy between the planetary amplitudes and the stellar variation, and that is not surprising given their very different time scales (Table 2).

Figure 4 shows the retrieved CPC amplitudes for the case where both planets are represented by our two-column model, as in Figure 2. The retrieved amplitudes for 'd' and 'b' are 29.0 ± 4.5 ppm and 12.7 ± 4.7 ppm, both in good agreement with their input values of 34.7 and 12.5 ppm, respectively. Compared to Figure 3, the 'd' amplitude is still degenerate with the orbital inclination, but the retrieved median value agrees with the 34.7 ppm input to 1.3σ . The retrieved 'b' amplitude (12.7 ± 4.7 ppm), is a marginal detection but in good agreement with the 12.5 ppm input value (see Figure 2). Regardless of the statistical significance of the 'b' amplitude, the comparison with 'd' would be very significant evidence for an atmosphere that is causing heat redistribution in the 'b' planet (otherwise the 'b' amplitude would be larger). That comparison assumes that the two planets are coplanar, as in the TRAPPIST-1 system (Gillon et al. 2017). An alternative would be a large difference in orbital inclination between the two planets. But a large inclination difference could be dynamically unstable (Livesey et al. 2024), and in any case would be a significant result in its own right.

6. DAY-TO-NIGHT TEMPERATURE CONTRAST

We envision CPCs detecting and characterizing rocky exoplanet atmospheres not by detecting spectral features, but by sensing the day-to-night temperature contrast, and inferring the requisite magnitude of heat transport (Seager & Deming 2009). By comparing the observed CPC amplitude with models, the magnitude of heat transport can in principle be determined. CPC amplitude varies with the albedo of the planet, as well as with the planetary radius and orbital inclination. Models such as our two-column model do not necessarily use heat transport and albedo as input parameters. Rather, those quantities are often determined self-consistently by the physics of the model, given starting boundary conditions such as the bulk composition of the atmosphere and the stellar irradiance. Hence

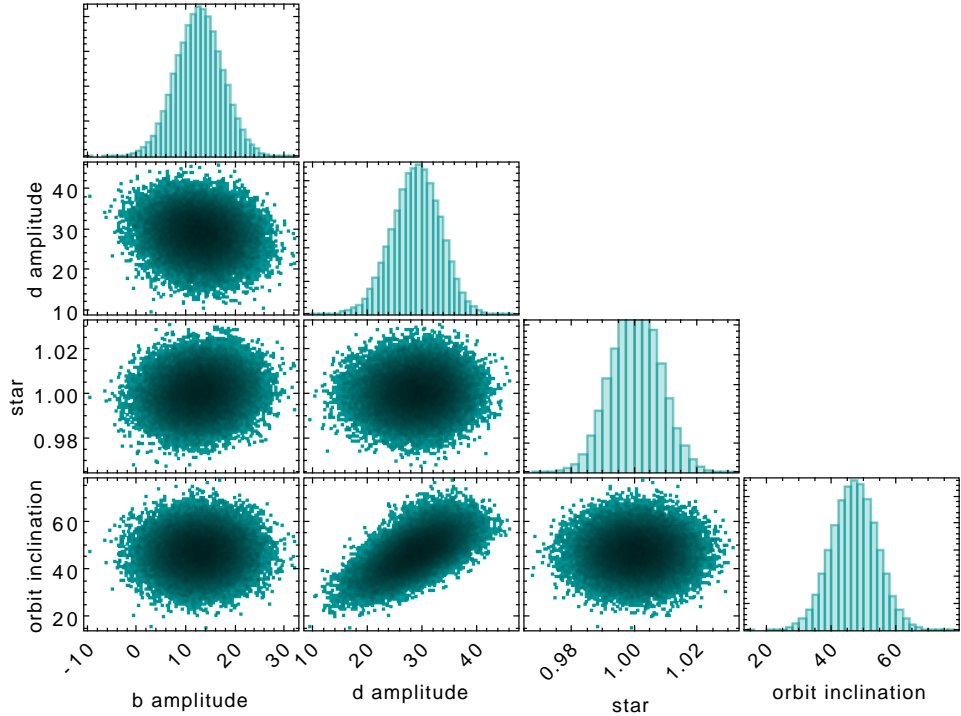


Figure 4. Corner plot for the sum of Proxima 'd', and 'b', assuming a hot rock model for 'd' (as in Figure 3), but using our two-column model for planet 'b'.

the first goal of observations is to infer the magnitude of the day-to-night variation in IR brightness temperature, independent of the planet's radius and orbital inclination. With that temperature contrast determined, in-depth physical models can be invoked to infer the magnitude of heat transport.

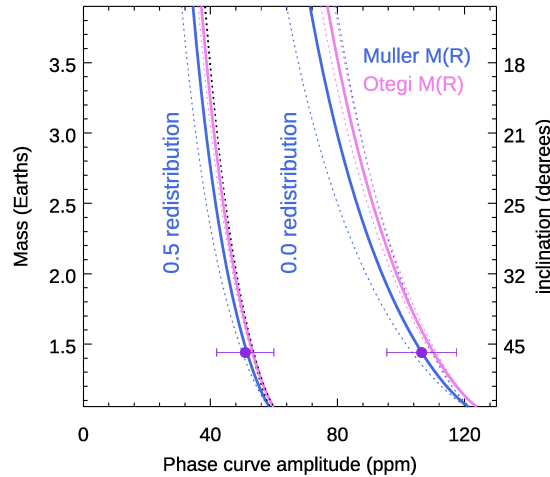


Figure 5. Possible mass and orbital inclination of Proxima Centauri b as a function of the amplitude of the CPC (21- vs. $12.8 \mu\text{m}$), where each curve is constrained by a mass radius relation. The phase curve amplitudes (X-axis) are based on the toy models from Kreidberg & Loeb (2016) (see text). We adopt $M(R)$ relations from Otegi et al. (2020) and Müller et al. (2024) in order to show that the result is not critically dependent on the exact form of $M(R)$. Dotted lines show the $\pm 1\sigma$ error ranges due to imprecision in $M(R)$. Because the curves for different values of heat redistribution are nearly vertical, an observed CPC amplitude will intersect only a small range of heat redistribution values (see text).

We here demonstrate that day-to-night temperature contrast, and consequently the magnitude of heat redistribution, can be determined without knowing the orbital inclination, by invoking a mass-radius relation. For this purpose, we use the toy models of [Kreidberg & Loeb \(2016\)](#), because they can specify the degree of heat redistribution as an input parameter. We determine the magnitude of heat redistribution by comparing the measured phase curve amplitude to models that are expressed in a quasi-inclination-independent form (Figure 5). Prior to implementing that quasi-inclination-independent form, we first consider the plausibility of the determination by invoking some general principles.

6.1. Plausibility of Measuring Heat Transport

First, we consider the number of physical variables that contribute to an observed CPC for the 2-planet Proxima system. Those are: R_b , R_d , i_b , i_d , ϵ_b , ϵ_d , α_b , and α_d , where R is radius, i is orbital inclination, ϵ is the fraction of incident energy transported to the night side (and re-emitted there), and α is the Bond albedo. Subscripts b and d refer to the two planets we consider in this system. At this point we have eight unknown variables, but only 4 observables: CPC amplitudes for each planet, and the radial velocity measurements of $M \sin i$ for each planet. By adopting a mass-radius relation (equivalent to an inclination-radius relation), and assuming that the orbital inclinations are the same (co-planar), we can reduce the number of unknowns to five, so the problem is still under-constrained. However, the under-constraint is not extreme, and models can be used to reduce the number of unknowns to equal the number of observables, as we now describe using a quasi-inclination-independent formulation.

6.2. A Quasi-inclination-independent Formulation

The inclination-independent form is achieved as follows: The RV data ($M \sin i$) imply orbital inclination as a function of possible mass, and a mass-radius relation ([Otegi et al. 2020](#); [Müller et al. 2024](#)) gives radii. For each value of heat redistribution, the models from [Kreidberg & Loeb \(2016\)](#) thereby predict phase curve amplitudes versus mass. Figure 5 plots those mass-amplitude relations, but with mass as the dependent variable. We use two versions of the mass-radius relation in order to demonstrate that the results are not strongly sensitive to the version of the mass-radius relation. The curves in Figure 5 are almost vertical because: 1) with increasing mass and radius, the phase curve amplitude in IR color increases, but 2) increasing mass requires smaller orbital inclinations and that works in the opposite direction.

For a given albedo, a measured phase curve amplitude (X-value on Figure 5), intersects only a small range of model curves that define the heat redistribution. In this form, the under-constrained aspect of the problem appears as the albedo. Fortunately, in the Rayleigh-Jeans limit the (Bond) albedo affects the phase curve amplitude only weakly. That occurs because the infrared flux is only linear (not exponential) versus temperature, and temperature is proportional to the fourth-root of the absorbed energy. Also, self-consistent physical models can be invoked to simultaneously determine consistency between the heat transfer and the albedo. In other words, the physical models connect the albedo and the heat transfer efficiency and provide the final relation that reduces the number of unknowns to equal the number of observables. Indeed, some possibilities can be constrained even without full modeling: for example the zero-redistribution curves on Figure 5 have sufficiently large amplitudes to require albedos not greatly exceeding 0.3.

7. THE LARGER POTENTIAL SAMPLE

Although we have emphasized Proxima b as the archetype of temperate rocky exoplanets, we emphasize that CPCs could be productive to detect and characterize atmospheres on a wide variety of exoplanets, including non-transiting ones, and including gaseous planets as well as rocky ones. Figure 6 shows the predicted $21 \mu\text{m}$ fluxes received at Earth for all exoplanets discovered by either transits or radial velocities, as a ratio to the flux predicted for Proxima b. Although Proxima b is the closest exoplanet, others can have greater fluxes if they have larger radii, and/or they are warmer.

Figure 6 color-codes planets with $21 \mu\text{m}$ fluxes exceeding 10% of Proxima b. Although some of our models for Proxima b are only marginally detectable (e.g., Figure 4), it is nevertheless reasonable to expect useful detections of some planets with lower predicted fluxes. The reasons are that the primary criterion is to be able to rule out the 'hot rock' case, and infer the existence of an atmosphere, even if that atmosphere does not produce a significant CPC amplitude (e.g., a planet with a spatially uniform temperature). The 'hot rock' cases will produce maximal CPC amplitudes. Also, other planetary systems may have orbital inclinations that are more favorable than Proxima's 47-degrees. Finally, we note that the signal-to-noise (S/N) for the photon-limited color measurements that we envision

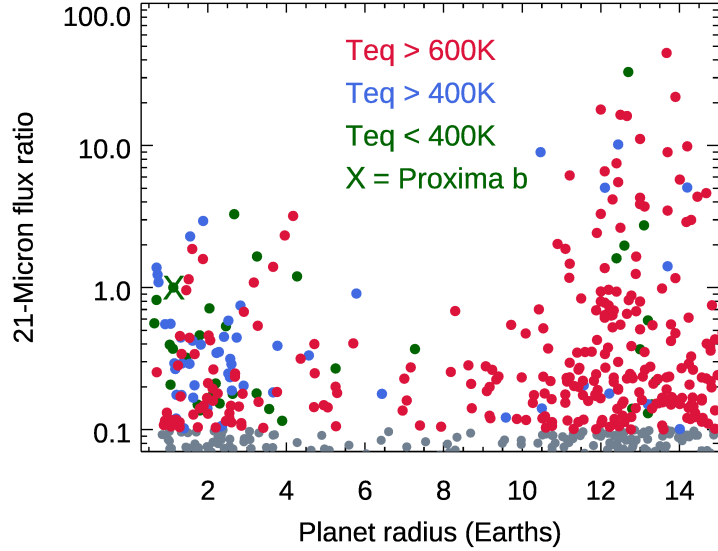


Figure 6. Predicted $21 \mu\text{m}$ flux for both transiting and non-transiting exoplanets, divided by the predicted flux from Proxima b, where the predicted fluxes are based on radii, distances, and equilibrium temperatures from *NexSci*^a. Points on the plot are color-coded by equilibrium temperature, and Proxima b is marked by the green X at the mid- to lower-left. Gray points at the bottom fall below the flux cutoff that we consider (see text). .

^a <https://exoplanetarchive.ipac.caltech.edu/cgi-bin/TblView/nph-tblView?app=ExoTbls&config=PSCompPars>

^b <https://exoplanetarchive.ipac.caltech.edu/cgi-bin/TblView/nph-tblView?app=ExoTbls&config=PSCompPars>

is proportional to the square root of flux, so that S/N does not degrade rapidly as flux decreases. Based on all of those considerations, we illustrate planets having flux ratios exceeding 0.1 in Figure 6. Those planets include many hot and warm gaseous planets (Jupiters to Neptunes) as well as additional temperate rocky planets. Considering the temperate range, we find 5 rocky planets (other than Proxima 'b' and 'd'). Those 5 are: Barnard e (Basant et al. 2025), GJ411 b (Díaz et al. 2019), Ross 128 b (Bonfils et al. 2018), YZ Ceti d (Astudillo-Defru et al. 2017), and Teegarden b (Zechmeister et al. 2019). They were all detected using radial velocity, and are not known to transit. They all orbit M-dwarf stars, and the activity of some host stars (especially flares) could be problematic for atmospheric detection and even for existence of planetary atmospheres (Garcia-Sage et al. 2017). However, not all M-dwarfs are active (e.g., Ross 128 is quiet, Bonfils et al. 2018), and the long-wave photometric capability of JWST gives us a powerful potential probe of these systems. One additional caveat is that the CPC analysis must know how the Earth-facing hemisphere of the planet varies with time. That is facilitated if we have high confidence that the planet's rotation is synchronous with the orbit.

We are reminded of early work that attempted to detect the atmospheres of close-in radial velocity planets prior to the discovery of transits. For example, both Charbonneau et al. (1999) and Collier Cameron et al. (1999) searched for reflected light from the non-transiting hot Jupiter Tau Bootis b. That pioneering work was quickly supplanted by the enormous productivity of transit observations. Meanwhile, observational capabilities have continued to improve on many fronts. Radial velocity observers are detecting numerous rocky planets, and most of them do not transit. Consequently, we suggest that there may be value in re-thinking alternate methods, and color phase curves are a potentially valuable option.

8. SUMMARY

In this paper, we develop and advocate an alternative method to detect and characterize exoplanetary atmospheres, emphasizing the importance for temperate rocky exoplanets. We have made these points:

- In §1 we point out that methods to measure the atmospheres of rocky exoplanets have focused on two methods: transit spectroscopy (e.g., the TRAPPIST-1 system), and secondary eclipse photometry. The challenges that these methods have encountered motivates additional approaches. For temperate planets, their planet-to-star flux observability peaks at long infrared wavelength, e.g. $21 \mu\text{m}$. We argue that the powerful exoplanet capa-

bility of JWST at those long wavelengths has been under-utilized for temperate planets. We thereby envision a third option that acquires and interprets long wavelength infrared photometry of an exoplanetary system in the ratio of two infrared wavelengths. We call this type of observation a color phase curve (CPC).

- §2 discusses that CPCs apply to non-transiting planets as well as to transiting planets, and the most natural application is to planets whose rotation is synchronous with their orbit. For temperate rocky planets, that will often imply that the host star is an M-dwarf. The observations we describe do not have to be continuous, rather they can be scheduled at intervals to sample peaks and valleys in the CPC, and we point out that radial velocity ephemerides are often sufficiently precise to schedule that sampling accurately. The version of CPCs that we envision uses near-continuum bands (JWST/MIRI 12.8- and 21 μm) to avoid possible degeneracies between spectral features and CPC amplitude. This formulation of a CPC will detect and characterize atmospheres via their heat transfer properties, not by detecting spectral features.
- We consider possible sources of interference and systematic error in §3. In §3.1, we point out that temperature variations due to spots and faculae on the host star will cancel in the ratio of two wavelengths in the Rayleigh-Jeans limit. Although real observations do not attain the Rayleigh-Jeans limit, the effect nevertheless greatly reduces stellar contamination due to spots and faculae. Moreover, stellar hosts often rotate at distinctly different time scales than the planetary orbit, further facilitating separation of stellar fluctuations from the CPC measurements. We also discuss the effect of stellar flares (§3.2), and the effect of possible changes in detector sensitivity in §3.3.
- In §4 we illustrate how CPCs will work using the example of the Proxima Centauri system. We simulated JWST/MIRI photometry for this system, using several models for the possible atmosphere of the 'b' planet. We demonstrate that the atmosphere, or lack thereof, would be detectable using a well designed JWST observational campaign in the ratio of 21-to 12.8 μm MIRI photometry. Simulating the data, we find that CPC amplitudes of both the 'b' and 'd' planets are detectable and can be separated from low-amplitude stellar rotational variations.
- We show in §6 that the atmospheric heat redistribution of a non-transiting planet can be determined without knowing the orbital inclination. That is possible by adopting a mass-radius relation, and by using constraints from self-consistent physical models.
- Beyond temperate rocky exoplanets, CPCs have application to a wide range of both transiting and non-transiting planets, and we discuss the relevant parameter space in §7. We point out that the radial velocity groups are detecting numerous new exoplanets down to the range of temperate rocky Earth-mass worlds, and most of them do not transit. New methods such as CPCs are needed to probe the atmospheres of those worlds.

REFERENCES

Alderson, L., Batalha, N. E., Wakeford, H. R., et al. 2024, *Astron.J.*, 167, 216, doi: [10.3847/1538-3881/ad32c9](https://doi.org/10.3847/1538-3881/ad32c9)

Anglada-Escudé, G., Amado, P. J., Barnes, J., et al. 2016, *Nature*, 536, 437, doi: [10.1038/nature19106](https://doi.org/10.1038/nature19106)

Artigau, É., Cadieux, C., Cook, N. J., et al. 2022, *Astron.J.*, 164, 84, doi: [10.3847/1538-3881/ac7ce6](https://doi.org/10.3847/1538-3881/ac7ce6)

Asplund, M. 2005, *ARAA*, 43, 481, doi: [10.1146/annurev.astro.42.053102.134001](https://doi.org/10.1146/annurev.astro.42.053102.134001)

Astudillo-Defru, N., Díaz, R. F., Bonfils, X., et al. 2017, *Astr.Ap.*, 605, L11, doi: [10.1051/0004-6361/201731581](https://doi.org/10.1051/0004-6361/201731581)

Basant, R., Luque, R., Bean, J. L., et al. 2025, *Ap.J.(Lett.)*, 982, L1, doi: [10.3847/2041-8213/adb8d5](https://doi.org/10.3847/2041-8213/adb8d5)

Bixel, A., & Apai, D. 2017, *Ap.J.(Lett.)*, 836, L31, doi: [10.3847/2041-8213/aa5f51](https://doi.org/10.3847/2041-8213/aa5f51)

Bonfils, X., Astudillo-Defru, N., Díaz, R., et al. 2018, *Astr.Ap.*, 613, A25, doi: [10.1051/0004-6361/201731973](https://doi.org/10.1051/0004-6361/201731973)

Boyajian, T. S., von Braun, K., van Belle, G., et al. 2012, *Ap.J.*, 757, 112, doi: [10.1088/0004-637X/757/2/112](https://doi.org/10.1088/0004-637X/757/2/112)

Cadieux, C., Doyon, R., MacDonald, R. J., et al. 2024, *Ap.J.(Lett.)*, 970, L2, doi: [10.3847/2041-8213/ad5afa](https://doi.org/10.3847/2041-8213/ad5afa)

Carlsson, M., Rutten, R. J., & Shchukina, N. G. 1992, *Astr.Ap.*, 253, 567

Charbonneau, D., & Gaudi, S. 2018, *Exoplanet Science Strategy* (The National Academies Press, Washington, DC), doi: [10.17226/25187](https://doi.org/10.17226/25187)

Charbonneau, D., Noyes, R. W., Korzennik, S. G., et al. 1999, *Ap.J.(Lett.)*, 522, L145, doi: [10.1086/312234](https://doi.org/10.1086/312234)

Collier Cameron, A., Horne, K., Penny, A., & James, D. 1999, *Nature*, 402, 751, doi: [10.1038/45451](https://doi.org/10.1038/45451)

Connors, N. J., Monaghan, C., Benneke, B., & Dang, L. 2025, *Ap.J.(Lett.)*, 989, L11, doi: [10.3847/2041-8213/adee0d](https://doi.org/10.3847/2041-8213/adee0d)

Crossfield, I. J. M., Hansen, B. M. S., Harrington, J., et al. 2010, *ApJ*, 723, 1436, doi: [10.1088/0004-637X/723/2/1436](https://doi.org/10.1088/0004-637X/723/2/1436)

Damasso, M., Del Sordo, F., Anglada-Escudé, G., et al. 2020, *Science Advances*, 6, eaax7467, doi: [10.1126/sciadv.aax7467](https://doi.org/10.1126/sciadv.aax7467)

Damiano, M., Bello-Arufe, A., Yang, J., & Hu, R. 2024, *Ap.J.(Lett.)*, 968, L22, doi: [10.3847/2041-8213/ad5204](https://doi.org/10.3847/2041-8213/ad5204)

Deming, D., Harrington, J., Seager, S., & Richardson, L. J. 2006, *Ap.J.*, 644, 560, doi: [10.1086/503358](https://doi.org/10.1086/503358)

Díaz, R. F., Delfosse, X., Hobson, M. J., et al. 2019, *Astr.Ap.*, 625, A17, doi: [10.1051/0004-6361/201935019](https://doi.org/10.1051/0004-6361/201935019)

Ducrot, E., Lagage, P.-O., Min, M., et al. 2025, *Nature Astronomy*, 9, 358, doi: [10.1038/s41550-024-02428-z](https://doi.org/10.1038/s41550-024-02428-z)

Espinoza, N., Allen, N. H., Glidden, A., et al. 2025, arXiv e-prints, arXiv:2509.05414, doi: [10.48550/arXiv.2509.05414](https://doi.org/10.48550/arXiv.2509.05414)

Espinoza, N., & Perrin, M. D. 2025, arXiv e-prints, arXiv:2505.20520, doi: [10.48550/arXiv.2505.20520](https://doi.org/10.48550/arXiv.2505.20520)

Fu, G., Welbanks, L., Deming, D., et al. 2024, *Nature*, 632, 752, doi: [10.1038/s41586-024-07760-y](https://doi.org/10.1038/s41586-024-07760-y)

Galuzzo, D., Berrilli, F., & Giovannelli, L. 2020, in *Journal of Physics Conference Series*, Vol. 1548, *Journal of Physics Conference Series* (IOP), 012012, doi: [10.1088/1742-6596/1548/1/012012](https://doi.org/10.1088/1742-6596/1548/1/012012)

Galuzzo, D., Cagnazzo, C., Berrilli, F., Fierli, F., & Giovannelli, L. 2021, *Ap.J.*, 909, 191, doi: [10.3847/1538-4357/abdeb4](https://doi.org/10.3847/1538-4357/abdeb4)

Garcia-Sage, K., Glocer, A., Drake, J. J., Gronoff, G., & Cohen, O. 2017, *Ap.J.(Lett.)*, 844, L13, doi: [10.3847/2041-8213/aa7eca](https://doi.org/10.3847/2041-8213/aa7eca)

Gilbert, E. A., Barclay, T., Kruse, E., Quintana, E. V., & Walkowicz, L. M. 2021, *Frontiers in Astronomy and Space Sciences*, 8, 190, doi: [10.3389/fspas.2021.769371](https://doi.org/10.3389/fspas.2021.769371)

Gillon, M., Ducrot, E., Bell, T. J., et al. 2025, arXiv e-prints, arXiv:2509.02128, doi: [10.48550/arXiv.2509.02128](https://doi.org/10.48550/arXiv.2509.02128)

Gillon, M., Triaud, A. H. M. J., Demory, B.-O., et al. 2017, *Nature*, 542, 456, doi: [10.1038/nature21360](https://doi.org/10.1038/nature21360)

Glidden, A., Ranjan, S., Seager, S., et al. 2025, arXiv e-prints, arXiv:2509.05407, doi: [10.48550/arXiv.2509.05407](https://doi.org/10.48550/arXiv.2509.05407)

Gordon, K. D., Sloan, G. C., Garcia Marin, M., et al. 2025, *Astron.J.*, 169, 6, doi: [10.3847/1538-3881/ad8cd4](https://doi.org/10.3847/1538-3881/ad8cd4)

Greene, T. P., Bell, T. J., Ducrot, E., et al. 2023, *Nature*, 618, 39, doi: [10.1038/s41586-023-05951-7](https://doi.org/10.1038/s41586-023-05951-7)

Gressier, A., Espinoza, N., Allen, N. H., et al. 2024, *Ap.J.(Lett.)*, 975, L10, doi: [10.3847/2041-8213/ad73d1](https://doi.org/10.3847/2041-8213/ad73d1)

Hu, R., Bello-Arufe, A., Zhang, M., et al. 2024, *Nature*, 630, 609, doi: [10.1038/s41586-024-07432-x](https://doi.org/10.1038/s41586-024-07432-x)

Jenkins, J. S., Harrington, J., Challener, R. C., et al. 2019, *MNRAS*, 487, 268, doi: [10.1093/mnras/stz1268](https://doi.org/10.1093/mnras/stz1268)

Kaufmann, P., Raulin, J.-P., de Castro, C. G. G., et al. 2004, *Ap.J.(Lett.)*, 603, L121, doi: [10.1086/383186](https://doi.org/10.1086/383186)

Kirk, J., Stevenson, K. B., Fu, G., et al. 2024, *Astron.J.*, 167, 90, doi: [10.3847/1538-3881/ad19df](https://doi.org/10.3847/1538-3881/ad19df)

Klein, B., Donati, J.-F., Hébrard, É. M., et al. 2021, *MNRAS*, 500, 1844, doi: [10.1093/mnras/staa3396](https://doi.org/10.1093/mnras/staa3396)

Knutson, H. A., Charbonneau, D., Allen, L. E., et al. 2007, *Nature*, 447, 183, doi: [10.1038/nature05782](https://doi.org/10.1038/nature05782)

Knutson, H. A., Madhusudhan, N., Cowan, N. B., et al. 2011, *Ap.J.*, 735, 27, doi: [10.1088/0004-637X/735/1/27](https://doi.org/10.1088/0004-637X/735/1/27)

Kreidberg, L., & Loeb, A. 2016, *Ap.J.(Lett.)*, 832, L12, doi: [10.3847/2041-8205/832/1/L12](https://doi.org/10.3847/2041-8205/832/1/L12)

Kreidberg, L., & Stevenson, K. B. 2025, arXiv e-prints, arXiv:2507.00933, doi: [10.48550/arXiv.2507.00933](https://doi.org/10.48550/arXiv.2507.00933)

Lim, O., Benneke, B., Doyon, R., et al. 2023, *Ap.J.(Lett.)*, 955, L22, doi: [10.3847/2041-8213/acf7c4](https://doi.org/10.3847/2041-8213/acf7c4)

Limbach, M. A., Vanderburg, A., Venner, A., et al. 2024, *Ap.J.(Lett.)*, 973, L11, doi: [10.3847/2041-8213/ad74ed](https://doi.org/10.3847/2041-8213/ad74ed)

Lincowski, A. P., Meadows, V. S., Zieba, S., et al. 2023, *Ap.J.(Lett.)*, 955, L7, doi: [10.3847/2041-8213/acee02](https://doi.org/10.3847/2041-8213/acee02)

Livesey, J. R., Barnes, R., & Deitrick, R. 2024, *ApJ*, 964, 4, doi: [10.3847/1538-4357/ad1ff4](https://doi.org/10.3847/1538-4357/ad1ff4)

Lustig-Yaeger, J., Fu, G., May, E. M., et al. 2023, *Nature Astronomy*, 7, 1317, doi: [10.1038/s41550-023-02064-z](https://doi.org/10.1038/s41550-023-02064-z)

Lustig-Yaeger, J., Sotzen, K. S., Stevenson, K. B., et al. 2025, *Ap.J.(Lett.)*, 994, L4, doi: [10.3847/2041-8213/ae17ae](https://doi.org/10.3847/2041-8213/ae17ae)

Mann, A. W., Feiden, G. A., Gaidos, E., Boyajian, T., & von Braun, K. 2015, *Ap.J.*, 804, 64, doi: [10.1088/0004-637X/804/1/64](https://doi.org/10.1088/0004-637X/804/1/64)

Maurin, A. S., Selsis, F., Hersant, F., & Belu, A. 2012, *Astr.Ap.*, 538, A95, doi: [10.1051/0004-6361/201117054](https://doi.org/10.1051/0004-6361/201117054)

May, E. M., MacDonald, R. J., Bennett, K. A., et al. 2023, *Ap.J.(Lett.)*, 959, L9, doi: [10.3847/2041-8213/ad054f](https://doi.org/10.3847/2041-8213/ad054f)

Meadows, V. S., & Crisp, D. 1996, *JGR*, 101, 4595, doi: [10.1029/95JE03567](https://doi.org/10.1029/95JE03567)

Meadows, V. S., Arney, G. N., Schwieterman, E. W., et al. 2018, *Astrobiology*, 18, 133, doi: [10.1089/ast.2016.1589](https://doi.org/10.1089/ast.2016.1589)

Moran, S. E., Stevenson, K. B., Sing, D. K., et al. 2023, *Ap.J.(Lett.)*, 948, L11, doi: [10.3847/2041-8213/accb9c](https://doi.org/10.3847/2041-8213/accb9c)

Müller, S., Baron, J., Helled, R., Bouchy, F., & Parc, L. 2024, *Astr.Ap.*, 686, A296, doi: [10.1051/0004-6361/202348690](https://doi.org/10.1051/0004-6361/202348690)

Newton, E. R., Mondrik, N., Irwin, J., Winters, J. G., & Charbonneau, D. 2018, *Astron.J.*, 156, 217, doi: [10.3847/1538-3881/aad73b](https://doi.org/10.3847/1538-3881/aad73b)

Otegi, J. F., Bouchy, F., & Helled, R. 2020, *Astr.Ap.*, 634, A43, doi: [10.1051/0004-6361/201936482](https://doi.org/10.1051/0004-6361/201936482)

Piaulet-Ghorayeb, C., Benneke, B., Turbet, M., et al. 2025, *Ap.J.*, 989, 181, doi: [10.3847/1538-4357/adf207](https://doi.org/10.3847/1538-4357/adf207)

Popinchalk, M., Faherty, J. K., Kiman, R., et al. 2021, *Ap.J.*, 916, 77, doi: [10.3847/1538-4357/ac0444](https://doi.org/10.3847/1538-4357/ac0444)

Rackham, B. V., Apai, D., & Giampapa, M. S. 2018, *Ap.J.*, 853, 122, doi: [10.3847/1538-4357/aaa08c](https://doi.org/10.3847/1538-4357/aaa08c)

Radica, M., Piaulet-Ghorayeb, C., Taylor, J., et al. 2025, *Ap.J.(Lett.)*, 979, L5, doi: [10.3847/2041-8213/ada381](https://doi.org/10.3847/2041-8213/ada381)

Ribas, I., Bolmont, E., Selsis, F., et al. 2016, *Astr.Ap.*, 596, A111, doi: [10.1051/0004-6361/201629576](https://doi.org/10.1051/0004-6361/201629576)

Savanov, I. S., & Dmitrienko, E. S. 2019, *INASAN Science Reports*, 3, 244, doi: [10.26087/INASAN.2019.3.1.038](https://doi.org/10.26087/INASAN.2019.3.1.038)

Scarsdale, N., Wogan, N., Wakeford, H. R., et al. 2024, *Astron.J.*, 168, 276, doi: [10.3847/1538-3881/ad73cf](https://doi.org/10.3847/1538-3881/ad73cf)

Seager, S., & Deming, D. 2009, *Ap.J.*, 703, 1884, doi: [10.1088/0004-637X/703/2/1884](https://doi.org/10.1088/0004-637X/703/2/1884)

Seager, S., & Shapiro, A. I. 2024, *Ap.J.*, 970, 155, doi: [10.3847/1538-4357/ad509a](https://doi.org/10.3847/1538-4357/ad509a)

Selsis, F., Wordsworth, R. D., & Forget, F. 2011, *Astr.Ap.*, 532, A1, doi: [10.1051/0004-6361/201116654](https://doi.org/10.1051/0004-6361/201116654)

Stevenson, K. B., et al. 2020, *Ap.J.(Lett.)*, 898, L35, doi: [10.3847/2041-8213/aba68c](https://doi.org/10.3847/2041-8213/aba68c)

Suárez Mascareño, A., Artigau, É., Mignon, L., et al. 2025, *Astr.Ap.*, 700, A11, doi: [10.1051/0004-6361/202553728](https://doi.org/10.1051/0004-6361/202553728)

Suárez Mascareño, A., Faria, J. P., Figueira, P., et al. 2020, *Astr.Ap.*, 639, A77, doi: [10.1051/0004-6361/202037745](https://doi.org/10.1051/0004-6361/202037745)

Swain, M. R., Pearson, K. A., Komacek, T. D., et al. 2025, *Ap.J.*, 982, 159, doi: [10.3847/1538-4357/adb835](https://doi.org/10.3847/1538-4357/adb835)

Teske, J. K., Wallack, N. L., Piette, A. A. A., et al. 2025, arXiv e-prints, arXiv:2509.17231. <https://arxiv.org/abs/2509.17231>

Vida, K., Oláh, K., Kővári, Z., et al. 2019, *Ap.J.*, 884, 160, doi: [10.3847/1538-4357/ab41f5](https://doi.org/10.3847/1538-4357/ab41f5)

Wargelin, B. J., Saar, S. H., Irving, Z. A., et al. 2024, *Ap.J.*, 977, 144, doi: [10.3847/1538-4357/ad8faa](https://doi.org/10.3847/1538-4357/ad8faa)

Weiner Mansfield, M., Xue, Q., Zhang, M., et al. 2024, *Ap.J.(Lett.)*, 975, L22, doi: [10.48550/arXiv.2408.15123](https://doi.org/10.48550/arXiv.2408.15123)

Xue, Q., Bean, J. L., Zhang, M., et al. 2024, *Ap.J.(Lett.)*, 973, L8, doi: [10.3847/2041-8213/ad72e9](https://doi.org/10.3847/2041-8213/ad72e9)

Yang, X., Cao, W., Wang, M., et al. 2025, *Ap.J.(Lett.)*, 988, L56, doi: [10.3847/2041-8213/adee95](https://doi.org/10.3847/2041-8213/adee95)

Zechmeister, M., Dreizler, S., Ribas, I., et al. 2019, *A&A*, 627, A49, doi: [10.1051/0004-6361/201935460](https://doi.org/10.1051/0004-6361/201935460)

Zieba, S., Kreidberg, L., Ducrot, E., et al. 2023, *Nature*, 620, 746, doi: [10.1038/s41586-023-06232-z](https://doi.org/10.1038/s41586-023-06232-z)